

# A Better Choice to Achieve High Volumetric Energy Density: Anode-Free Lithium-Metal Batteries

Liangdong Lin, Kun Qin, Yong-sheng Hu, Hong Li, Xuejie Huang, Liumin Suo,\* and Liquan Chen

Volumetric energy density is a critical but easily neglected index of lithium-metal batteries (LMBs). Compared with gravimetric energy density, the volumetric energy density (VED) of LMBs is much more sensitive to the anode/cathode (A/C) ratio due to the low density of lithium (Li) metal and the volume expansion of the Li-metal anode owing to its pulverization during cycles. Anode-free LMBs (AF-LMBs) have high theoretical VED due to the absence of an anode and high retention with relatively low cell expansion. Because Li plating highly depends on the mother substrate, Li plating on copper (Cu) substrates is more reversible and denser than that on Li substrates during cycling, which is beneficial for maintaining high volumetric capacity and efficient Li utilization. Therefore, considering that excess Li must be strictly limited to achieve competitive energy density, AF-LMBs (with bare Cu foil as the anode current collector) for high-volumetric-density batteries are recommended.

## 1. Introduction

Lithium-metal batteries (LMBs) can achieve high gravimetric energy density (GED) owing to the high theoretical gravimetric capacity of lithium (Li) metal ( $3860 \text{ Ah kg}^{-1}$ ).<sup>[1]</sup> Thus, most studies on LMBs employ significantly excess Li to achieve long cycle life,<sup>[2]</sup> ignoring its negative effect on the volumetric energy density (VED) because VED is more sensitive to the anode/cathode (A/C) ratio than GED. The theoretical volumetric capacity of Li metal ( $2060 \text{ Ah L}^{-1}$ ) is less than three times that

of lithiated graphite ( $\text{LiC}_6$ ) ( $719 \text{ Ah L}^{-1}$ ) due to the low density of Li ( $0.534 \text{ g cm}^{-3}$ );<sup>[3]</sup> thus, LMBs lose their advantages on VED over Li-ion batteries (LIB) when the A/C ratio exceeds to 2.87 (Figure 1a and Table S1, Supporting Information).<sup>[3]</sup> Besides, Li plating on the anode side causes unacceptable volume expansion, and even idealized Li plating causes nearly 20% cell expansion (LIBs  $\approx 1.5\%$ ).<sup>[4]</sup> In addition, Li anodes process pulverization in practice, leading to high surface areas and porosities,<sup>[1e,5]</sup> where the porosity factor of plated Li easily exceeds 50%, significantly aggravating the expansion and lowering the VEDs of LMBs than anticipated (Figure 1b and Table S2, Supporting Information).

Furthermore, higher cell expansion lowers Li utilization efficiency. This is because large expansion results from highly porous Li plating, which is more conducive to side reactions between Li and electrolytes, forming more solid electrolyte interphases (SEIs)<sup>[1f,6]</sup> and aggravating the irreversible loss of electrolytes and active Li (Figure 1c). Moreover, stripping such high-surface-area Li is susceptible to electrical disconnection, forming isolated dead Li,<sup>[7]</sup> which further accelerates cell failure. Therefore, in applications, it is challenging for LMBs to achieve reversibly dense Li plating during cycles that directly determine VEDs and cell expansion.

Herein, we recommend anode-free LMBs (AF-LMBs) constructed with bare Cu foil as the anode current collector to achieve high initial VED with the minimum A/C ratio of 1. More importantly, AF-LMBs can maintain high VED throughout the charge–discharge process by producing less expansion because Li nucleation and plating on Cu substrates are much denser than those on Li substrates (Figure 1d). This is further discussed in a later section. Besides, without using highly reactive metallic Li,<sup>[3,5,8]</sup> AF-LMBs have advantages over LMBs in cell fabrication and cost.<sup>[9]</sup>

To clarify the above viewpoint, we focused on AF-LMBs and their advantage in VEDs and volume expansion. The differences between Li plating on Cu substrates (AF-LMB) and Li substrates (LMB) have been studied by in situ optical microscopy (OM) and scanning electron microscopy (SEM),<sup>[10]</sup> revealing denser Li plating on Cu substrates. Meanwhile, the cell expansion of AF-LMB and LMB pouch cells during cycling has been monitored by in situ pressure sensors,<sup>[3,11]</sup> which confirmed that the high-surface-area plating of Li on Li substrates

L. Lin, K. Qin, Y.-s. Hu, H. Li, X. Huang, L. Suo, L. Chen  
Beijing Advanced Innovation Center for Materials Genome Engineering  
Key Laboratory for Renewable Energy  
Beijing Key Laboratory for New Energy Material and Devices  
Beijing National Laboratory for Condensed Matter Physics  
Institute of Physics  
Chinese Academy of Science  
Beijing 100190, China  
E-mail: suoliumin@iphy.ac.cn

L. Lin, K. Qin, L. Suo  
Center of Materials Science and Optoelectronics Engineering  
University of Chinese Academy of Sciences  
Beijing 100049, China  
L. Suo  
Yangtze River Delta Physics Research Center Co. Ltd.  
Liyang 213300, China

 The ORCID identification number(s) for the author(s) of this article can be found under <https://doi.org/10.1002/adma.202110323>.

DOI: 10.1002/adma.202110323

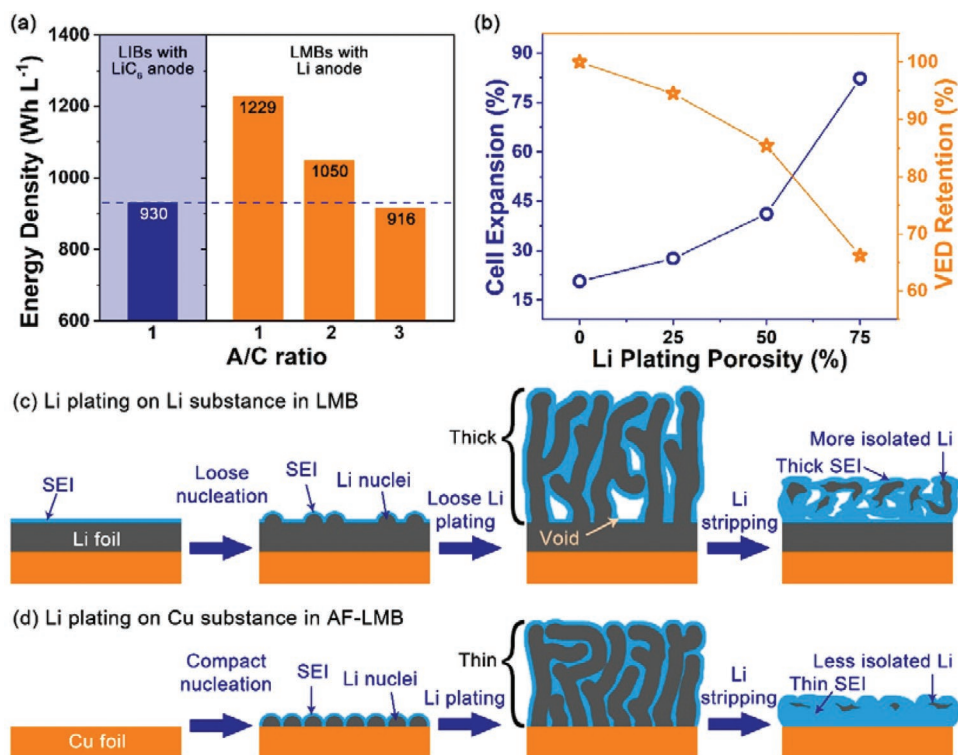


**Figure 1.** Challenges to the practical application of LMBs. a) Influence of the A/C ratio on VEDs. b) Impact of Li plating porosity on cell expansion and VEDs. c,d) Illustration of Li plating on a Li substrate in an LMB (c) and a Cu substrate in an AF-LMB (d).

increases cell thickness and decreases VED.<sup>[8d,e,12]</sup> Thus, the VED of the AF-LMB assembled herein (976 Wh L<sup>-1</sup>) is much higher than that of LMB (846 Wh L<sup>-1</sup>), but their GEDs are equal. Furthermore, AF-LMB outperforms LMB in VED retention after cycling without significant volume expansion caused by further pulverization of the dense Li foil. Besides, the denser Li plating morphology on the Cu substrate can reduce SEI and dead Li formation, which enhances efficient Li utilization, further highlighting the advantage of AF-LMBs.

## 2. Results and Discussion

To obtain the volumetric capacities of Li plating on different substrates, the changes in the thickness of Li plating on Cu and Li substrates were monitored in situ using pressure sensors and assisted by SEM imaging. According to Hooke's law, there is a linear relationship between the change in thickness ( $\Delta H$ ) and change in pressure ( $\Delta P$ ) ( $\approx 4.9 \text{ N } \mu\text{m}^{-2}$ , Figure S1, Supporting Information), and the  $\Delta H$  of a cell can be calculated based on  $\Delta P$ . Due to the high volume expansion caused by Li plating, the slight change in the volume of LiNi<sub>0.8</sub>Co<sub>0.1</sub>Mn<sub>0.1</sub>O<sub>2</sub> (NCM) cathode and other cell components is negligible (Table S3, Supporting Information),<sup>[3,7,11,13]</sup> and the  $\Delta H$  of the entire cell is approximately the  $\Delta H$  of the Li anode. NCM, as the Li source for the first charge, can provide 5.58 mAh cm<sup>-2</sup> Li (first discharge: 5 mAh cm<sup>-2</sup>), as shown in Figure 2a,b. The cells were evaluated using an ether-based electrolyte (6 m lithium bis(fluorosulfonyl)imide (LiFSI) in 1,2-dimethoxyethane (DME) (LiFSI-DME), which can simultaneously satisfy wide enough

electrochemical stability window and superior reversibility of the Li-metal anode.<sup>[5,8c]</sup> During the process, Li plating on the Li substrate showed higher  $\Delta H$  (86.33  $\mu\text{m}$ ) than that on the Cu substrate (59.39  $\mu\text{m}$ ) by providing more remarkable  $\Delta P$  (423 and 291 N for Li and Cu substrates, respectively; Figure 2a,b). Such a high difference reveals that Li plating on a Cu substrate is much denser than on a Li substrate, attributed to the excellent kinetics of Li nucleation on Cu substrates, as confirmed by the lower overpotential of Li nucleation at the initial Li plating (the inset of Figure 2a,b). The kinetics of Li plating highly depends on the mother substrate. Previous studies have shown that (110) facet of Li plating exhibits much better electrochemical reversibility than the (200) facet, which is dominant for commercial Li foils.<sup>[14]</sup> Besides, the SEI formed on Cu substrate contains more inorganic components (especially LiF) than that on Li substrate, which has been proved to be more conducive to the efficient cycling of Li anode.<sup>[5,15]</sup> Figures S2–S4 (Supporting Information) show that Li plating on a Cu substrate grows as large 3D particle sizes with a preferential crystal orientation of (110), which not only lowers the porosity of Li anodes to ensure dense Li plating but also improves the reversibility of Li anodes.

Notably, the initial state of a Li substrate is in bulk with minimized volume, but as the cycle progresses, it is gradually utilized and pulverized into loose dead Li,<sup>[16]</sup> accelerating volume expansion.<sup>[17]</sup> Therefore, volume growth on Li substrates after cycles (17.9  $\mu\text{m}$ ) is more significant than that on Cu substrates (6.53  $\mu\text{m}$ , Figure 2c), resulting in a continuous loss of volumetric capacity. Thus, herein, freshly plated Li on a Cu substrate showed not only higher volumetric capacity

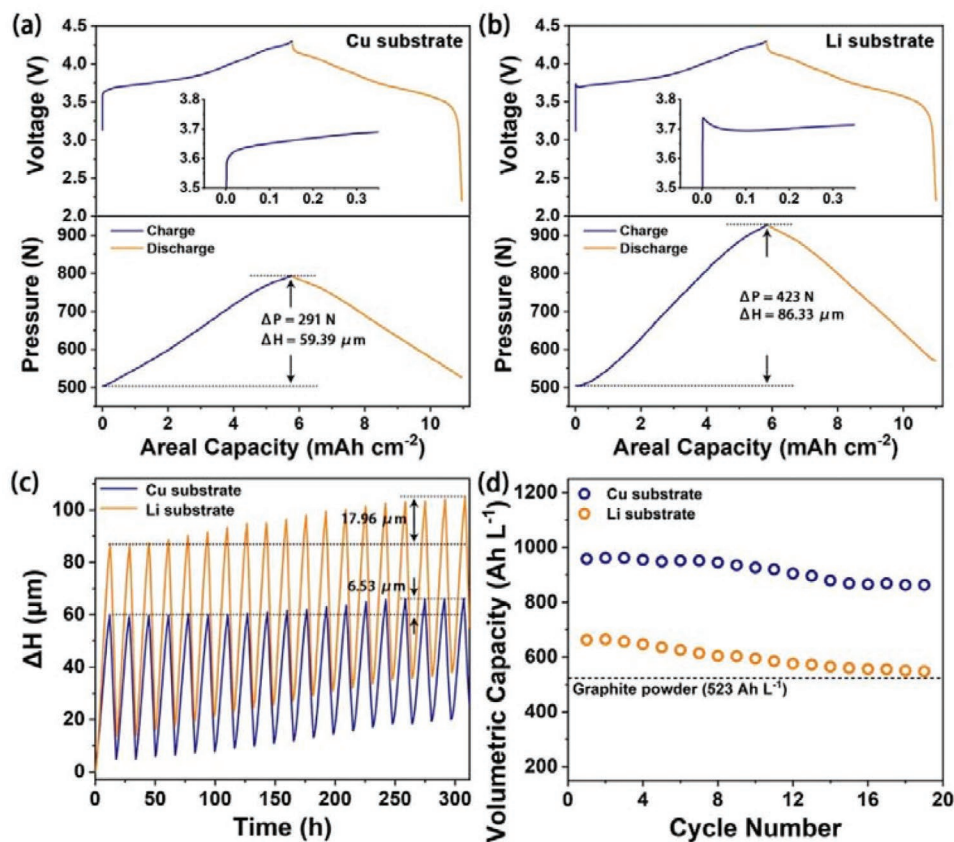


**Figure 2.** Volumetric capacities of Li anodes. a,b) Voltage profiles and the corresponding pressure profiles of NCM cells with Cu (a) and Li (b) substrates as anode current collectors. c)  $\Delta H$  versus time profiles of Li cycling on Cu and Li substrates. d) Volumetric capacities of freshly plated Li on Cu and Li substrates.

(961 Ah L<sup>-1</sup>) but also higher capacity retention (90.08%) than those on a Li substrate (665 Ah L<sup>-1</sup>, 82.65%) (Figure 2d). Moreover, the volumetric capacity of Li cycling on Li substrate after 19 cycles almost has no advantage over that of graphite powder with a porosity of 27% (550 vs 523 Ah L<sup>-1</sup>). Therefore, the application of Li foil needs to be more cautious.

In addition to the electrochemical results, microscopy images of Li plating on Cu and Li substrates were obtained (Figure 3). To compare the plating behavior of Li on Cu and Li substrates in situ, half of the Cu plate was covered with a Li foil (Figure 3a). Then, Li was plated on a hybrid electrode (Video S1, Supporting Information). Different Li nucleation behavior was observed from the cross-sectional OM image of the hybrid electrode after 20 s Li plating (Figure 3b). The nucleation of Li on the Cu substrate was more uniform, and the surface of the Cu substrate was uniformly covered by Li nuclei, whereas Li nuclei on the Li substrate surface were loosely distributed like islands. Further growth of the island-like Li nuclei on the Li substrate resulted in the formation of high-surface-area Li plating morphology accompanied by many voids and isolated Li, as shown in the cross-sectional OM image after 5 min Li plating (Figure 3c).

A similar phenomenon was observed in the SEM images after Li plating. As shown in Figure 3d, after 0.25 mAh cm<sup>-2</sup> Li plating, the surface of the Cu substrate was evenly covered by

plated Li, whereas there were still several uncovered parts on the surface of Li substrate with even dendritic Li. When the amount of Li plating increased to 5 mAh cm<sup>-2</sup> (Figure 3e), the surface of the Li substrate was completely covered by plated Li but still not as dense as that plated on the Cu substrate. The cross-sectional SEM images of Li plating (Figure 3f and Figure S4, Supporting Information) show that the nucleation and growth of Li on Li substrates were loose and porous. Notably, the denser plating of Li on Cu substrate can be observed in a variety of other commonly used electrolytes (Figure S5, Supporting Information).<sup>[14,16,18]</sup> And the nondense Li plating behavior on the Li substrate compared with that on the Cu substrate at room temperature has been theoretically predicted by Schnell and Røe using density functional theory and molecular dynamics simulations.<sup>[19]</sup> Such high-surface-area morphology is more conducive to side reactions between Li and an electrolyte, forming more SEI and consuming precious active Li. The stripping of dendritic Li is susceptible to electrical disconnection, forming isolated dead Li, further increasing the irreversible Li loss. Furthermore, high-surface-area Li plating on a Li substrate increases electrode thickness and decreases volumetric capacity.

Li plating morphology impacts Coulombic efficiencies (CEs). The CE of Li cycling on the Cu substrate can be easily obtained from Cu/Li cells.<sup>[20]</sup> However, it is difficult to quantify the CE of Li plating/stripping on Li substrates since additional Li on a Li



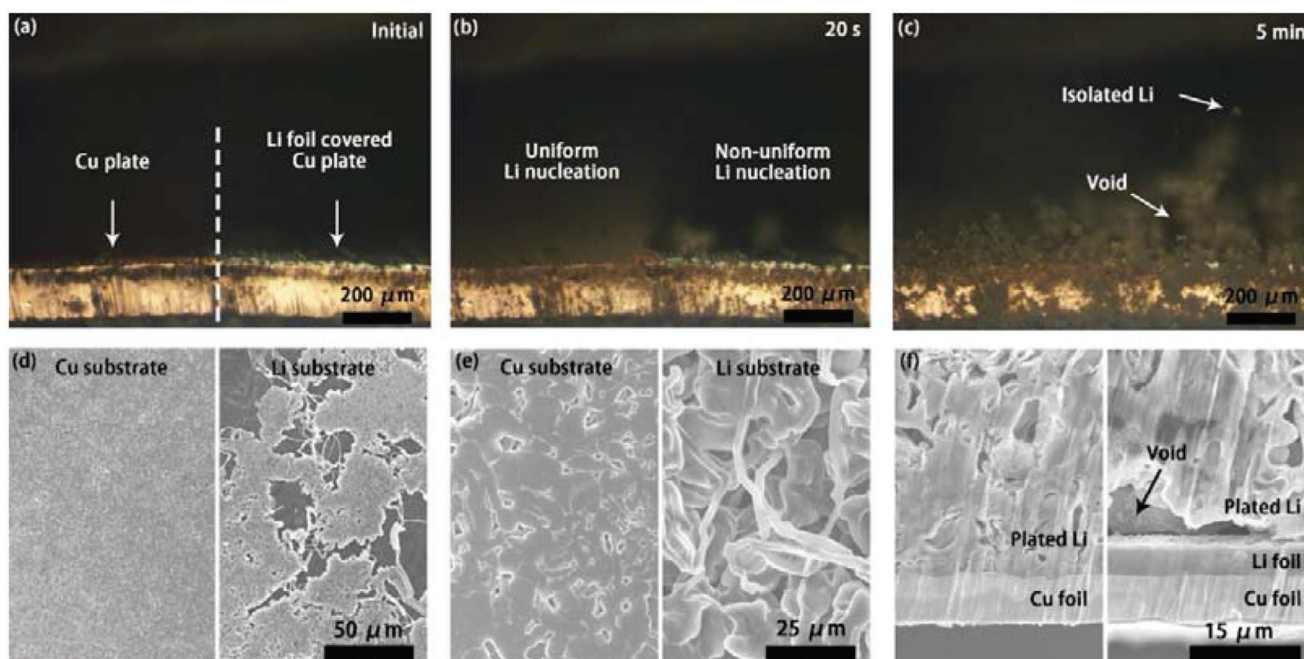


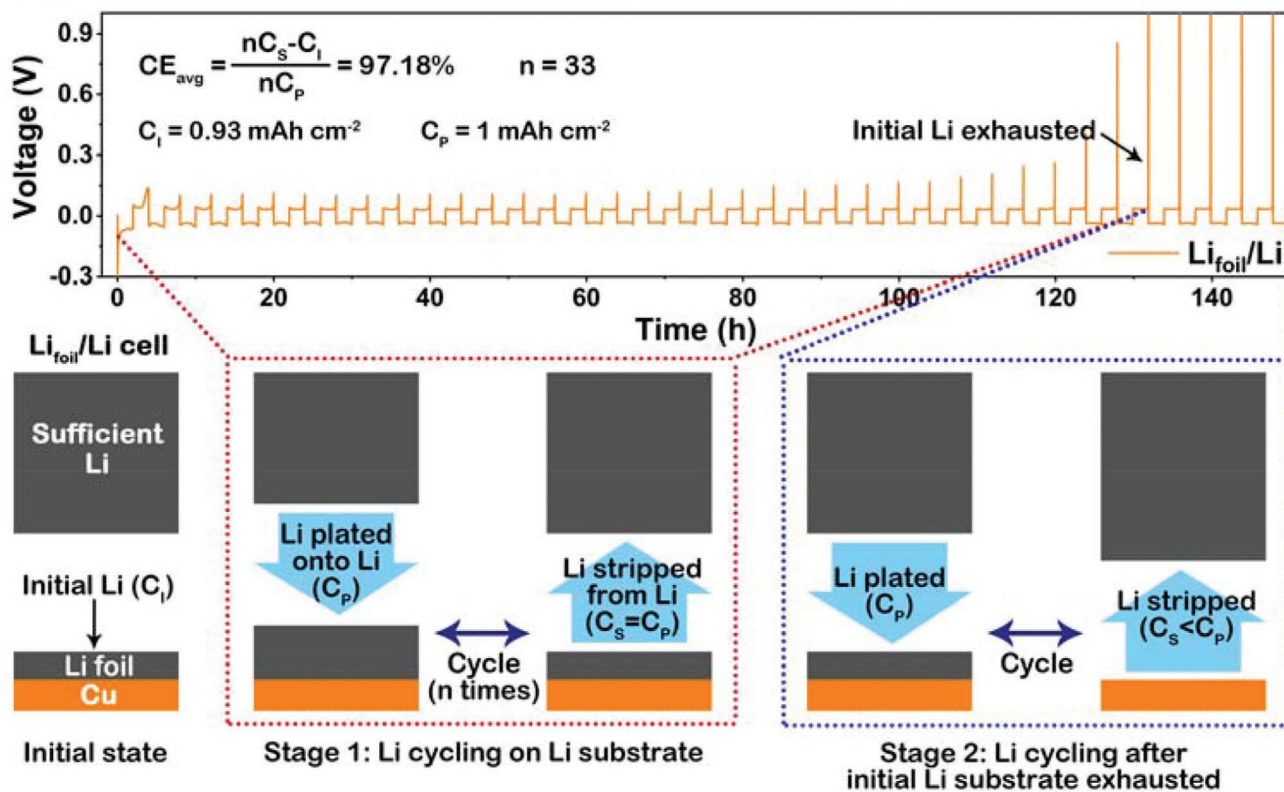
**Figure 3.** Morphologies of Li plating on Cu and Li substrates. a) Cross-sectional OM images of pristine Cu (left) and Li (right) substrates. b,c) Cross-sectional OM images of Cu and Li substrates after 20 s (b) and 5 min (c) of Li plating. d,e) SEM images of Cu (left) and Li (right) substrates after 0.25 mAh cm<sup>-2</sup> (d) and 5 mAh cm<sup>-2</sup> (e) of Li plating. f) Cross-sectional SEM images of Cu (left) and Li (right) substrates after 5 mAh cm<sup>-2</sup> of Li plating.

substrate can offset the irreversible Li loss during Li cycling.<sup>[20,21]</sup> Herein, to quantify the CE of Li cycling on the Li substrate, Li<sub>foil</sub>/Li cell was assembled using an ultrathin Li foil on Cu foil (containing 0.93 mAh cm<sup>-2</sup> Li sources measured through Li stripping experiments in Figure S6 in the Supporting Information with a standard deviation of 0.00876, Supporting Information) as the Li<sub>foil</sub> working electrode and Li plate (500 μm) as the Li counter electrode (Figure 4a). The cell was cycled by the first 1 mAh cm<sup>-2</sup> Li plating (C<sub>p</sub>) onto the Li<sub>foil</sub> working electrode and then stripping the newly plated Li off (C<sub>s</sub>). In the first stage, Li sources pre-existing on the Li<sub>foil</sub> electrode could compensate for the irreversible Li loss during Li cycling, resulting in C<sub>s</sub> = C<sub>p</sub>. In the 33rd cycle, the pre-existing Li was exhausted (Figure 4a), and the stripping of Li from the working electrode could no longer be cut off with a fixed capacity of 1 mAh cm<sup>-2</sup>, but it was cut off as the voltage increased to 1 V (C<sub>s</sub> < C<sub>p</sub>). At the moment, the amount of total Li loss on the Li<sub>foil</sub> working electrode was equal to the amount of initial pre-existing Li (C<sub>1</sub> = 0.93 mAh cm<sup>-2</sup>). Therefore, Li plating/stripping on the Li substrate after 33 cycles irreversibly consumed 0.93 mAh cm<sup>-2</sup> Li with an average CE of 97.18% (Figure 4a, in the ether-based electrolyte). In contrast, Li loss on the Cu substrate could be obtained by accumulating the CEs of a Cu/Li cell. Thus, the Cu substrate consumed 0.50 mAh cm<sup>-2</sup> Li in 33 cycles with a higher average CE of 98.49% (Figure 4b), indicating higher Li utilization efficiency on the Cu substrate than that on the Li substrate. It should be noted that although the LiFSI-DME electrolyte we used here is one of the most advanced electrolytes reported so far, the change of the current-collector will still lead to a huge difference in the Li plating behavior and efficiency. A similar phenomenon was observed in the carbonate-based electrolyte (1 M LiPF<sub>6</sub> in a mixture of ethylene carbonate (EC) and

diethyl carbonate (DEC) (v:v = 1:1)), as shown in Figures S7 and S8 (Supporting Information). Moreover, Cu/Li cells could work properly with higher current density and capacity, whereas Li<sub>foil</sub>/Li cells could not (Figures S9–S12, Supporting Information), further highlighting the advantages of Cu substrates. Therefore, it is necessary to be more cautious when selecting the anode current-collector of LMBs. Any material that is more lithiophilic and can achieve denser Li plating helps to increase the VED of LMBs, which deserves to be vigorously developed instead of Li abuse.

ΔH in pouch cells was also monitored to obtain the VED of AF-LMB and LMB (Figure 5 and Figure S13, Supporting Information). A new class of Li-rich NCM (Li<sub>2</sub>NCM, Li<sub>2</sub>Ni<sub>0.8</sub>Co<sub>0.1</sub>Mn<sub>0.1</sub>O<sub>2</sub>) cathode was employed in the AF-LMB.<sup>[8c]</sup> The total amount of extra Li in the Li-rich NCM cathode was controlled as much as the Li<sub>foil</sub> in LMB to ensure the same GED for the AF-LMB and LMB. The extra Li in the Li-rich NCM cathode can be released during the first charge to supplement the Li loss. As shown in Figure S14 (Supporting Information), an obvious new plateau appeared at 2.4 V during the first charge of the Li-rich NCM/Cu cell, corresponding to the release of additional Li, 1.28 mAh cm<sup>-2</sup> more than that of the NCM/Li<sub>foil</sub> cell. After completing the Li supplementation, the Li-rich NCM can convert into conventional NCM and continue to participate in cell cycling function as a cathode. This process will also reduce the volume of the cathode by ≈5.5%, which appropriately alleviates the volume expansion during cell charging. Benefiting from the denser Li plating on the Cu foil, the Li-rich NCM/Cu cell exhibited a smaller ΔP than NCM/Li<sub>foil</sub> cell (359 N vs 423 N, Figure S14, Supporting Information and Figure 2b) even with higher capacity. Both Li-rich NCM/Cu and NCM/Li<sub>foil</sub> showed comparable initial GED and cycle stability

(a) CE of Li cycling on Li substrate



(b) CE of Li cycling on Cu substrate

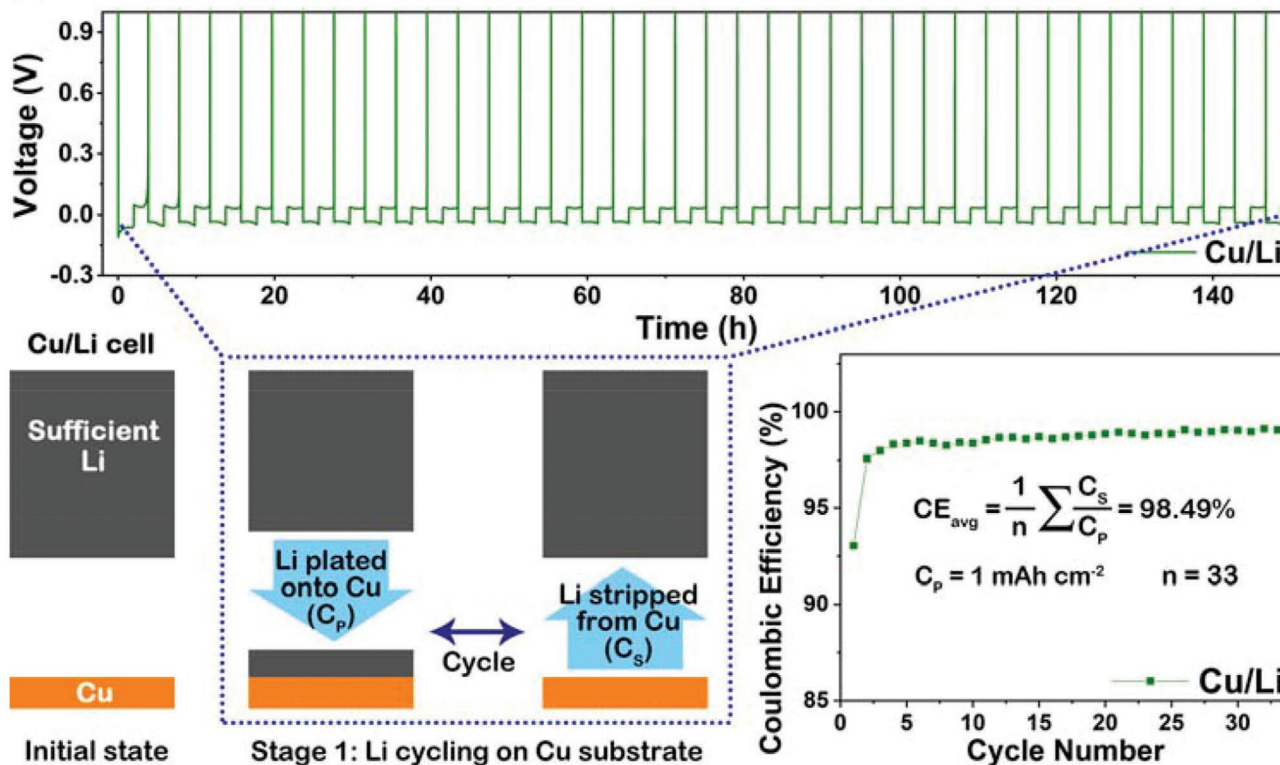
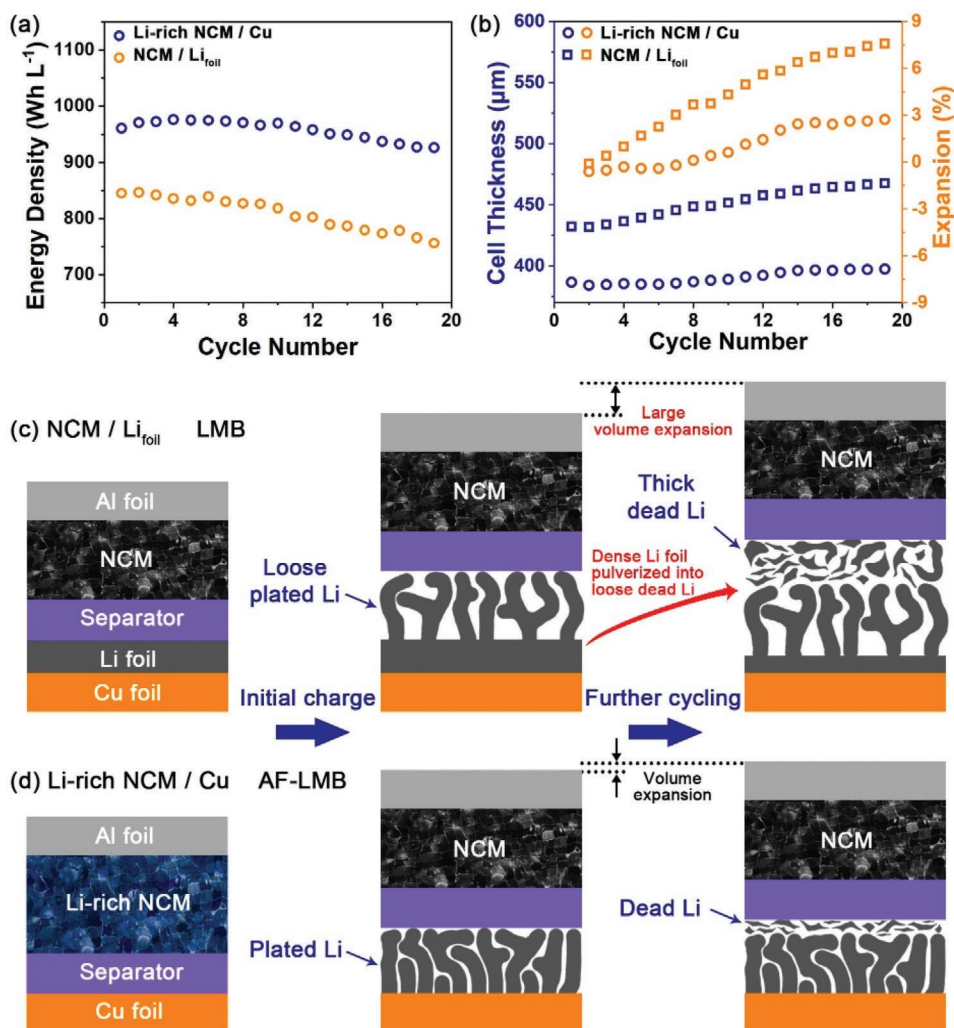


Figure 4. Li utilization efficiencies on Cu and Li substrates. a) Voltage versus time profile of a Li<sub>foil</sub>/Li cell and corresponding illustration of Li cycling on a Li substrate. b) Voltage versus time profile of Cu/Li cell and corresponding illustration and CE of Li cycling on a Cu substrate.





**Figure 5.** VEDs of LMB and AF-LMB at 100% stage-of-charge (SOC). a) VEDs of a Li-rich NCM/Cu AF cell and NCM/Li<sub>foil</sub> cell. b) Cell thicknesses and expansion ratios of a Li-rich NCM/Cu AF cell and NCM/Li<sub>foil</sub> cell. c) Volume expansion in NCM/Li<sub>foil</sub> LMB. d) Volume expansion in Li-rich NCM/Cu AF-LMB.

after 100 cycles (Figures S15, S16, and Table S4, Supporting Information). Li-rich NCM/Cu cell exhibits higher capacity retention than NCM/Li<sub>foil</sub> cell due to the higher Li utilization efficiency on Cu substrates. However, comparing their VEDs, the energy density of Li-rich NCM/Cu is 976 Wh L<sup>-1</sup>, which is much higher than the 846 Wh L<sup>-1</sup> for NCM/Li<sub>foil</sub> (Figure 5b and Table S5, Supporting Information), showing the advantage of AF-LMBs in terms of VED. Notably, even with similar GEDs, the VEDs of cells may be highly different, which highlights that the VED is an important parameter that should not be ignored.

The pre-existing Li foil in LMBs suffers from continuously pulverizing into high-surface-area dead Li, further increasing volume expansion (Figure 5b,c). Therefore, volume expansion in NCM/Li<sub>foil</sub> with cycles is more severe than that of Li-rich NCM/Cu (Figure 5b), resulting in a continuous and rapid decrease in VED (Figure 5a). In contrast, the anode-free design in AF-LMB (Li-rich NCM/Cu) prevents the continuous volume expansion caused by further pulverization of Li foil, which helps to maintain the VED during the entire cycle life (Figure 5b,d). Thus, the Li-rich NCM/Cu cell exhibited lower

expansion (2.7%) and higher VED retention (96.4%) than the NCM/Li<sub>foil</sub> cell (7.6% and 89.5%, respectively).

### 3. Conclusions

AF-LMBs have high initial VED and low volume expansion during cycling, resulting in high VED. First, the Li-metal-free cell design in AF-LMBs exhibits a much higher VED (975 Wh L<sup>-1</sup>) than that of LMB (846 Wh L<sup>-1</sup>). Second, Li plates are much denser in AF-LMB than in LMB, ensuring high VED during cycling. Third, Li utilization on a Cu substrate is more efficient than that on Li substrate, where Li nucleation is more uniform, and the growth is much denser, effectively preventing irreversible Li loss resulting from the formation of SEI and dead Li. Finally, AF-LMBs have low volume expansion without continuous pulverization of the Li foil in LMBs, which is favorable to maintain the VED. Based on these results, AF-LMBs are promising for the further development of high-energy batteries.

## Supporting Information

Supporting Information is available from the Wiley Online Library or from the author.

## Acknowledgements

This work was supported by the Center for Clean Energy, the Youth Fund of National Natural Science Foundation of China (22109174), and the China Postdoctoral Science Foundation (2019M660845).

## Conflict of Interest

The authors declare no conflict of interest.

## Data Availability Statement

The data that support the findings of this study are available from the corresponding author upon reasonable request.

## Keywords

anode-free batteries, cell expansion, lithium-metal batteries, porosity, volumetric energy density

Received: December 17, 2021

Revised: March 20, 2022

Published online: May 4, 2022

- [1] a) M. Armand, J. M. Tarascon, *Nature* **2008**, 451, 652; b) J. B. Goodenough, Y. Kim, *Chem. Mater.* **2010**, 22, 587; c) B. Dunn, H. Kamath, J.-M. Tarascon, *Science* **2011**, 334, 928; d) J. W. Choi, D. Aurbach, *Nat. Rev. Mater.* **2016**, 1, 16013; e) D. Lin, Y. Liu, Y. Cui, *Nat. Nanotechnol.* **2017**, 12, 194; f) P. Albertus, S. Babinec, S. Litzelman, A. Newman, *Nat. Energy* **2018**, 3, 16.
- [2] a) N. Li, Y. Yin, C. Yang, Y. Guo, *Adv. Mater.* **2016**, 28, 1853; b) Y. Chong, X.-B. Cheng, Y. Yao, X. Shen, B.-Q. Li, W.-J. Li, R. Zhang, J.-Q. Huang, H. Li, Q. Zhang, *Adv. Mater.* **2018**, 30, 1804461; c) L. Lin, F. Liang, K. Zhang, H. Mao, J. Yang, Y. Qian, *J. Mater. Chem. A* **2018**, 6, 15859; d) X. Liang, Q. Pang, I. R. Kochetkov, M. S. Sempere, H. Huang, X. Sun, L. F. Nazar, *Nat. Energy* **2017**, 2, 17119; e) L. Lin, J. Wang, R. Li, C. Wang, C. Zhang, J. Yang, Y. Qian, *Energy Storage Mater.* **2020**, 26, 112; f) Y. Gao, Y. Zhao, Y. C. Li, Q. Huang, T. E. Mallouk, D. Wang, *J. Am. Chem. Soc.* **2017**, 139, 15288; g) E. Cha, M. D. Patel, J. Park, J. Hwang, V. Prasad, K. Cho, W. Choi, *Nat. Nanotechnol.* **2018**, 13, 337.
- [3] A. J. Louli, M. Genovese, R. Weber, S. G. Hames, E. R. Logan, J. R. Dahn, *J. Electrochem. Soc.* **2019**, 166, A1291.
- [4] M. Bauer, M. Wachtler, H. Stöwe, J. V. Persson, M. A. Danzer, *J. Power Sources* **2016**, 317, 93.
- [5] L. Lin, L. Suo, Y.-S. Hu, H. Li, X. Huang, L. Chen, *Adv. Energy Mater.* **2021**, 11, 2003709.
- [6] S. S. Zhang, *ACS Appl. Energy Mater.* **2018**, 1, 910.
- [7] M. Genovese, A. J. Louli, R. Weber, C. Martin, T. Taskovic, J. R. Dahn, *J. Electrochem. Soc.* **2019**, 166, A3342.
- [8] a) S. Nanda, A. Gupta, A. Manthiram, *Adv. Energy Mater.* **2020**, 11, 2000804; b) J. Qian, B. D. Adams, J. Zheng, W. Xu, W. A. Henderson, J. Wang, M. E. Bowden, S. Xu, J. Hu, J.-G. Zhang, *Adv. Funct. Mater.* **2016**, 26, 7094; c) L. Lin, K. Qin, Q. Zhang, L. Gu, L. Suo, Y.-S. Hu, H. Li, X. Huang, L. Chen, *Angew. Chem., Int. Ed.* **2021**, 60, 8289; d) A. J. Louli, A. Eldesoky, R. Weber, M. Genovese, M. Coon, J. deGooyer, Z. Deng, R. T. White, J. Lee, T. Rodgers, R. Petibon, S. Hy, S. J. H. Cheng, J. R. Dahn, *Nat. Energy* **2020**, 5, 693; e) R. Weber, M. Genovese, A. J. Louli, S. Hames, C. Martin, I. G. Hill, J. R. Dahn, *Nat. Energy* **2019**, 4, 683.
- [9] a) J.-G. Zhang, *Nat. Energy* **2019**, 4, 637; b) B. J. Neudecker, N. J. Dudney, J. B. Bates, *J. Electrochem. Soc.* **2000**, 147, 517; c) S. S. Zhang, X. L. Fan, C. S. Wang, *Electrochim. Acta* **2017**, 258, 1201; d) S. S. Zhang, X. Fan, C. Wang, *Electrochem. Commun.* **2018**, 89, 23.
- [10] L. Suo, W. Xue, M. Gobet, S. G. Greenbaum, C. Wang, Y. Chen, W. Yang, Y. Li, J. Li, *Proc. Natl. Acad. Sci. USA* **2018**, 115, 1156.
- [11] A. J. Louli, L. D. Ellis, J. R. Dahn, *Joule* **2019**, 3, 745.
- [12] M. Genovese, A. J. Louli, R. Weber, S. Hames, J. R. Dahn, *J. Electrochem. Soc.* **2018**, 165, A3321.
- [13] A. O. Kondrakov, A. Schmidt, J. Xu, H. Geßwein, R. Mönig, P. Hartmann, H. Sommer, T. Brezesinski, J. Janek, *J. Phys. Chem. C* **2017**, 121, 3286.
- [14] Q. Zhao, Y. Deng, N. W. Utomo, J. Zheng, P. Biswal, J. Yin, L. A. Archer, *Nat. Commun.* **2021**, 12, 6034.
- [15] Y. Xu, H. Wu, H. Jia, M. H. Engelhard, J.-G. Zhang, W. Xu, C. Wang, *Nano Energy* **2020**, 76, 105040.
- [16] C. Niu, D. Liu, J. A. Lochala, C. S. Anderson, X. Cao, M. E. Gross, W. Xu, J.-G. Zhang, M. S. Whittingham, J. Xiao, J. Liu, *Nat. Energy* **2021**, 6, 723.
- [17] H. Kim, G. Jeong, Y. U. Kim, J. H. Kim, C. M. Park, H. J. Sohn, *Chem. Soc. Rev.* **2013**, 42, 9011.
- [18] a) S. Chen, J. Zheng, D. Mei, K. S. Han, M. H. Engelhard, W. Zhao, W. Xu, J. Liu, J.-G. Zhang, *Adv. Mater.* **2018**, 30, 1706102; b) L. Yu, S. Chen, H. Lee, L. Zhang, M. H. Engelhard, Q. Li, S. Jiao, J. Liu, W. Xu, J.-G. Zhang, *ACS Energy Lett.* **2018**, 3, 2059; c) X.-Q. Zhang, X.-B. Cheng, X. Chen, C. Yan, Q. Zhang, *Adv. Funct. Mater.* **2017**, 27, 1605989; d) X. Fan, L. Chen, X. Ji, T. Deng, S. Hou, J. Chen, J. Zheng, F. Wang, J. Jiang, K. Xu, C. Wang, *Chem* **2018**, 4, 174; e) L. Suo, Y.-S. Hu, H. Li, M. Armand, L. Chen, *Nat. Commun.* **2013**, 4, 1481; f) H.-H. Sun, A. Dolocan, J. A. Weeks, R. Rodriguez, A. Heller, C. B. Mullins, *J. Mater. Chem. A* **2019**, 7, 17782; g) X. Fan, L. Chen, O. Borodin, X. Ji, J. Chen, S. Hou, T. Deng, J. Zheng, C. Yang, S.-C. Liou, K. Amine, K. Xu, C. Wang, *Nat. Nanotechnol.* **2018**, 13, 715.
- [19] I. T. Røe, S. K. Schnell, *J. Mater. Chem. A* **2021**, 9, 11042.
- [20] W. Li, H. Yao, K. Yan, G. Zheng, Z. Liang, Y.-M. Chiang, Y. Cui, *Nat. Commun.* **2015**, 6, 7436.
- [21] a) J. C. Burns, L. J. Krause, D. B. Le, L. D. Jensen, J. R. Dahn, *J. Electrochem. Soc.* **2011**, 158, A1417; b) C.-J. Huang, B. Thirumalraj, H.-C. Tao, K. N. Shitaw, H. Sutiono, T. T. Hagos, T. T. Beyene, L.-M. Kuo, C.-C. Wang, S.-H. Wu, W.-N. Su, B. J. Hwang, *Nat. Commun.* **2021**, 12, 1452.